Numerical Simulation of Orographic Enhancement of Rain with a Mesoscale Model

Evelyne Richard, Nadine Chaumerliac, Jean Francois Mahfouf, Everett Nickerson

Numerical Simulation of Orographic Enhancement of Rain with a Mesoscale Model

EVELYNE RICHARD, NADINE CHAUMERLIAC AND JEAN FRANCOIS MAHFOUF

Laboratoire Associé de Météorologie Physique, Université de Clermont-Ferrand II, 63170 Aubière, France

EVERETT C. NICKERSON

National Oceanic and Atmospheric Administration, Air Resources Laboratory, GMCC, Boulder, CO 80303

(Manuscript received 19 May 1986, in final form 18 October 1986)

ABSTRACT

Orographic precipitation enhancement associated with the feeder–seeder mechanism proposed by Bergeron has been simulated using a two dimensional model based upon primitive equations including detailed parameterized microphysics. A case-by-case comparison is made between model results and each of 14 well-documented precipitation episodes in southern Wales. The model reproduces the observed strong dependence of the precipitation enhancement on the low-level wind speed, as well as the weak dependence on the upwind precipitation rate. Model results also demonstrate that a satisfactory treatment of orographically enhanced precipitation requires the linking of the dynamical, thermodynamical and microphysical processes.

1. Introduction

Orographic enhancement of rain via the feeder–seeder mechanism, first put forward by Bergeron (1965), has been studied theoretically and experimentally by several authors (Storebo, 1976; Bader and Roach, 1977; Carruthers and Choularton, 1983). This mechanism, according to which raindrops from upper-level (seeder) clouds wash out small droplets within low-level (feeder) orographic clouds, appears to be very efficient in increasing the surface rainfall rate (Hill et al., 1981, hereafter referred to as HBB). Radar observations and automatic raingage data obtained by HBB during the course of a field project carried out in southern Wales showed that 80% of the enhancement occurred in the first 1.5 km above the hills. This enhancement was very dependent upon the wind velocity, v_L, and almost independent of the upwind rainfall rate, P_0. Numerical simulations performed by (HBB) with the theoretical washout model of Bader and Roach (1977; hereafter referred to as BR), for the actual values of v_L and P_0 encountered during the observational program showed a much smaller dependence of the enhancement on v_L and a much larger dependence on P_0 than observed.

Carruthers and Choularton (1983) subsequently thought to resolve differences between theory and observation by computing the orographic enhancements over a bell shaped mountain using a three-layer stratified airflow model, a potential flow model, and the model of BR. They found that the BR airflow formulation gave inaccurate results because of an overestimation of streamline displacement over the hill. But even with the stratified airflow model, the high sensitivity to the wind speed was not reproduced by the computations. Gocho (1978) used a simplified airflow model with highly detailed microphysics to study the sensitivity of the enhancement to various microphysical parameters.

In all of these models, the representation of the simulated airflow may be questionable because the diabatic heating is usually neglected. Carruthers and Choularton introduced diabatic heating in the stratified airflow model by replacing the cloudy regions with a region of reduced stability. However, that approach supposes that the cloud boundaries are known a priori and may lead to non-self-consistent solutions for the actual moist flows.

Our approach was to use a two-dimensional computer model which integrates the equations of motion governing the flow of moist air over a topographic barrier. Comparisons to analytical solutions or other model results have shown that this model can accurately represent linear hydrostatic mountain waves as well as nonlinear ones (Nickerson et al., 1986). This approach allows us to study a wide variety of situations which are not amenable to analytic solutions (i.e., non linear, terrain of arbitrary shape, etc.), and it also allows a more accurate treatment of the moist processes.

2. Model formulation

The model used is the two-dimensional version of Nickerson et al. (1986). It links the dynamical, thermodynamical and microphysical processes, thereby permitting interaction and feedback between warm cloud microphysics processes and the temperature,

moisture and wind fields. The ice phase is not taken into account since our region of interest will be located below the melting level. We will recall here only some aspects of the microphysical parameterizations necessary for the understanding of this paper.

a. Microphysics

The microphysics are described by three prognostic variables: $q = q_v + q_{cw}$, the sum of water vapor and cloud water mixing ratios; q_{rw}, the rainwater mixing ratio; and N_{rw}, the raindrop total number concentration. The corresponding equations take the following form:

$$\frac{dq}{dt} = -Q_{\text{aut}} - Q_{\text{acc}} + Q_{\text{eva}} \tag{1}$$

$$\frac{dq_{rw}}{dt} = +Q_{\text{aut}} + Q_{\text{acc}} - Q_{\text{eva}} + Q_{\text{sed}} \tag{2}$$

$$\frac{dN_{rw}}{dt} = +N_{\text{aut}} - N_{\text{self}} + N_{\text{sed}} \tag{3}$$

where Q and N stand for the various sources or sinks of mixing ratio and concentration, respectively. The subscript "aut" is for autoconversion of cloud droplets into raindrops, "acc" is for accretion of cloud droplets by raindrops and "self" for the self-collection of the raindrops. The subscripts "eva" and "sed" are related to the rain evaporation and sedimentation, respectively (see Nickerson et al., 1986, for the details of these terms.).

The cloud water mixing ratio, q_{cw}, is diagnosed from the predicted value of q. In the event of supersaturation with respect to liquid water, excess vapor is converted into cloud water. Rainwater is assumed to be distributed log-normally with diameter. That is,

$$dN_{rw} = \frac{N_{rw}}{\sqrt{2\pi}\sigma_r D} \exp\left[-\frac{1}{2\sigma_r^2}\ln^2\left(\frac{D}{D_{0r}}\right)\right] dD \tag{4}$$

is the number of raindrops in the size range D to $D + dD$. Here, σ_r and D_{0r} are distribution parameters. Only one of them can be diagnosed given q_{rw} and N_{rw}. We close the microphysical system of equations by assuming a constant value of σ_r and computing D_{0r}. For the model runs reported below, $\sigma_r = 0.5$. The conversion rates of cloud droplets to raindrops (Q_{aut}, N_{aut}) are computed according to the parameterizations of Berry and Reinhardt (1973). Since the present model does not include an explicit formulation for the cloud spectra, it is not possible to calculate directly the mean mass of the cloud droplets ($x_{fc} = \rho_a q_{cw}/N_{cw}$) or the cloud spectrum variance (var$x$) needed in the parameterizations. To evaluate the autoconversion rate, we assume that the cloud droplets are also partitioned according to a lognormal distribution, for which the distribution parameters σ_c and D_{0c} remain constant. This is equivalent to supposing that x_{fc} and var$x$ remain constant in Berry and Reinhardt's parameterizations.

b. Initial conditions

In BR, the terrain is represented by a 40 km slope leading to a 400 m high plateau. As mentioned by HBB, however, Glamorgan hill's terrain (location of their study) is steeper. We therefore take for the terrain a slope of 1 in 40 (as recommended by HBB) instead of 1 in 100.

The horizontal grid length is set to 8 km and the model domain extends to 200 km. Vertically, it contains 15 levels equally spaced in the ν coordinate system (modified σ system), and the top of the domain is located at 100 mb.

The model is initialized with a radiosounding taken from HBB. During the course of the simulation, the feeder cloud is generated by the orographic forcing while the seeder cloud is represented through a specified resulting precipitation rate, P_s, introduced at a given vertical level, k_s. This is done in sedimentation terms of Eqs. (2) and (3) defined by

$$Q_{\text{sed}} = \frac{\partial S_q}{\partial z}, \tag{5}$$

$$N_{\text{sed}} = \frac{\partial S_N}{\partial z}, \tag{6}$$

where S_q and S_N are the sedimentation fluxes related to q_{rw} and N_{rw} respectively.

At the seeding level, k_s, S_q is replaced by

$$S'_q = S_q + \frac{\rho_w P_s}{\rho_a}. \tag{7}$$

With the parameterization used in the model, the ratio S_q/S_N is a function of the mean rain diameter $\overline{D_r}$:

$$\frac{S_q}{S_N} = \alpha(\overline{D_r}). \tag{8}$$

Assuming that this relation is also valid for the seeding raindrops, we then obtain

$$S'_N = S_N + \frac{\rho_w P_s}{\rho_a \alpha(\overline{D_{sr}})}, \tag{9}$$

where $\overline{D_{sr}}$ is the mean diameter of the seeding raindrops.

3. Sensitivity tests

A series of nine simulations were carried out to test the sensitivity of the model results to the assumed values of the microphysical parameters. In addition to specifying the seeding precipitation rate, P_s, we must specify the cloud distribution parameters, σ_c and D_{0c}, the seeding raindrops mean diameter, $\overline{D_{sr}}$, and the vertical level, k_s, (or its equivalent height, z_s) at which seeding occurs. The different cases and the corresponding values of the microphysical parameters are listed in Table 1.

TABLE 1. Computed cases for the sensitivity tests.

Expt no.	σ_c	$\bar{D}_c$ (μm)	Z_s (km)	P_s (mm h^{-1})	$\bar{D}_{sr}$ (μm)
1	0.16	20		No seeding	
2	0.28	40			
3	0.16	20	1.5	3	100
4	0.28	40	1.5	3	100
5	0.28	40	1.5	2	100
6	0.28	40	2.2	2	100
7	0.28	40	1.5	4	100
8	0.28	40	1.5	4	300
9	0.28	40	1.5	4	500

Besides the aforementioned tests dealing with the microphysical parameterization, two more processes are considered: the role of the dynamical/microphysical interaction and the effect of evaporation of the raindrops. These two physical processes are often neglected in other studies, but may affect the precipitation reaching the ground.

All the sensitivity experiments were performed with the radiosounding from case 1 in HBB, and the results are displayed after 4 h of integration.

a. Cloud spectrum parameters

The cloud distribution parameters may have a great influence on the resulting precipitation. A cloud distribution centered on large cloud droplets will produce more rainwater than a cloud distribution with a small model diameter. As an example, we present in Fig. 1 the results of two experiments without seeding but with two different cloud spectra: a continental case with $\sigma_c = 0.16$ and $\bar{D}_c = 20$ μm, and a maritime case defined by $\sigma_c = 0.28$ and $\bar{D}_c = 40$ μm. For the continental case, the orographic cloud has a maximum value of 0.68 g kg^{-1} for the cloud water mixing ratio, but it is almost nonprecipitating (0.01 g kg^{-1} for the maximum rainwater mixing ratio). On the other hand, the maritime cloud attains a much higher rainwater mixing ratio (0.46 g kg^{-1}), but with a corresponding cloud water mixing ratio of only 0.16 g kg^{-1}. The maximum precipitation rates at the ground are 2.2 and 0.06 mm h^{-1} for the maritime and continental spectrum respectively.

The same two experiments have been redone with a seeding precipitation rate of 3 mm h^{-1} introduced at about 1.5 km above the ground. As can be seen in Fig. 2, although the structure of the rainwater mixing ratio fields and the rain concentration fields are different from one simulation to the other, the precipitation patterns of these two simulations are nearly identical. In the continental case, the rain comes mainly from the seeding raindrops growing by accretion, and the maximum of rainwater mixing ratio is just below the seeding level. With the maritime cloud spectrum, the rain reaching the ground comes, on the one hand, from the conversion of the orographic cloud water into raindrops, and, on the other hand, from the seeding raindrops which this time cannot grow as much by accretion because less cloud water is available. In this case, the maximum rainwater mixing ratio found near the

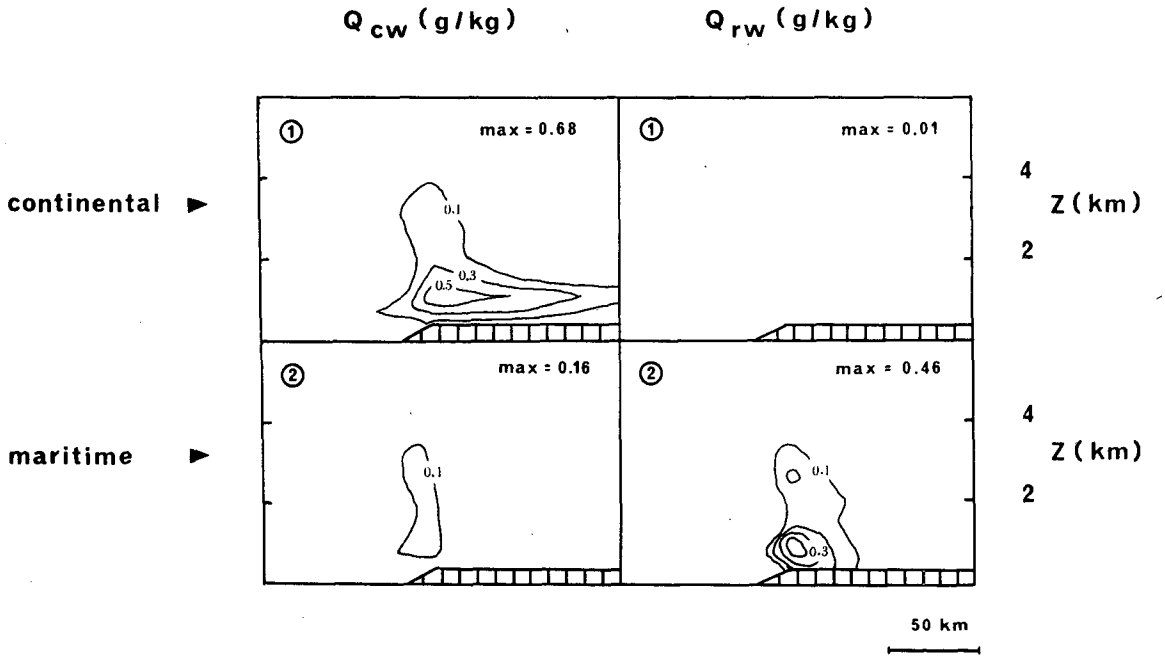

FIG. 1. Cloud water and rainwater mixing ratio fields for continental and maritime cloud spectrum in the absence of seeding from above. The circled number in the left corner designates the experiment number (see Table 1). In the right corner the maximum value is plotted.

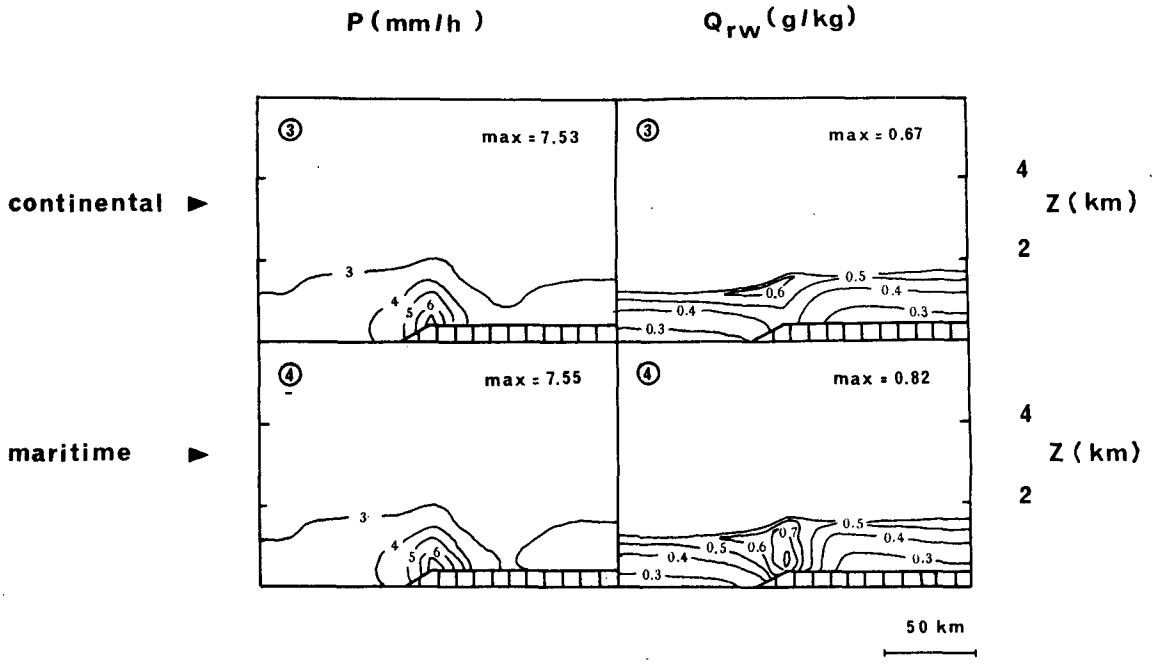

FIG. 2. Precipitation rate and rainwater mixing ratio fields for continental and maritime cloud spectrum with a seeding rate of 3 mm h^{-1}.

ground is higher than in the continental case but is carried by smaller drops (443 μm for the maximum rain mean diameter versus 601 μm for the continental case); hence the similarity of the rainfall rates. Another experiment, which utilized cloud spectrum parameters $\sigma_c = 0.22$ and $\overline{D}_c = 35$ μm gave similar results for the precipitation field.

Gocho (1978) found that the maximum rainfall rate tends to become large as the size of the generated cloud droplets increases, but his tests were made using a constant conversion rate. Due to the assumptions made in our parameterization, any change in the cloud spectrum will modify the conversion rate. For the purpose of this study, the results shown in Fig. 2 indicate that

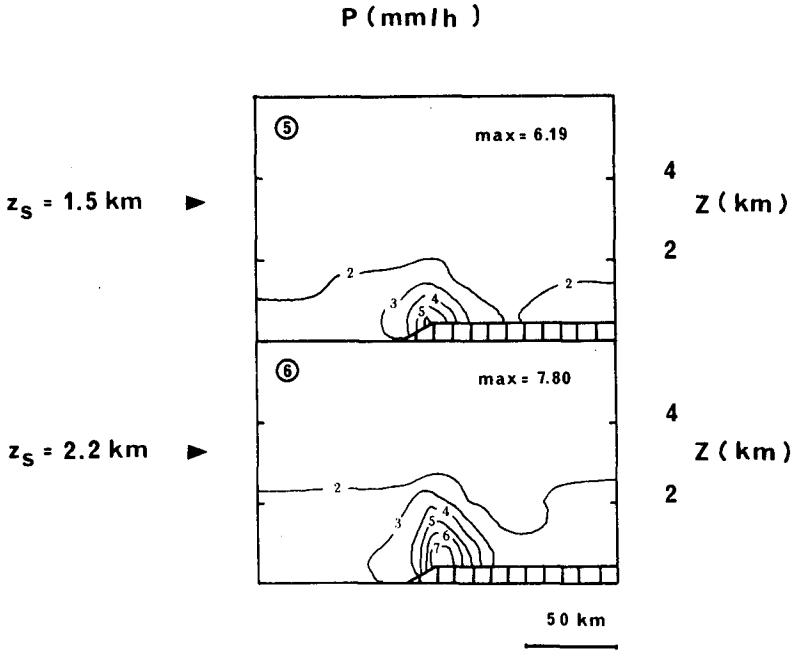

FIG. 3. Precipitation rate fields for two different heights of seeding, z_s.

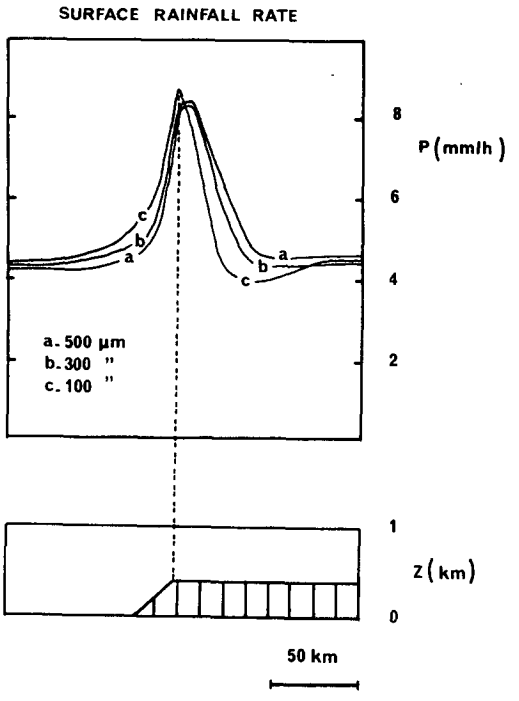

FIG. 4. Surface rainfall rate for different values of the mean seeding raindrop diameter, $\overline{D_{sr}}$.

an incorrect specification of the cloud spectrum will not significantly affect the computed orographic enhancement of rainfall in the presence of upper level seeding.

b. *Seeding height*

Experiments 5 and 6 were performed with a maritime cloud spectrum. In both cases the seeding precipitation rate was 2 mm h^{-1}. The seeding was introduced at about 2.2 km above the ground for experiment 5 and at about 1.5 km for experiment 6.

Increasing the seeding height significantly increases the precipitation maximum (6.2 mm h^{-1} for experiment 5 and 7.8 mm h^{-1} for experiment 4) and moves it downwind (see Fig. 3). This effect is explained by the fact that for the case 1 sounding, the orographic cloud top reaches 3 km. With a seeding height of 1.5 km, the seeding raindrops do not wash out the entire depth of the orographic cloud.

c. *Seeding rain mean diameter*

Keeping all other parameters constant (maritime cloud spectrum, P_s = 4 mm h^{-1}, z_s = 1.5 km), we varied $\overline{D_{sr}}$ from 100 μm to 300 and 500 μm for experiments 7, 8 and 9, respectively. This variation has little impact on the surface precipitation (see Fig. 4). Increasing the seeding rain mean diameter, $\overline{D_{sr}}$, should lead to a more efficient washout because the volume swept out by an individual raindrop is larger. On the other hand, for a given seeding precipitation rate, P_s, an increase in $\overline{D_{sr}}$ decreases the number concentration of seeding raindrops and thus should yield a less efficient washout. These two effects seem somehow to compensate each other.

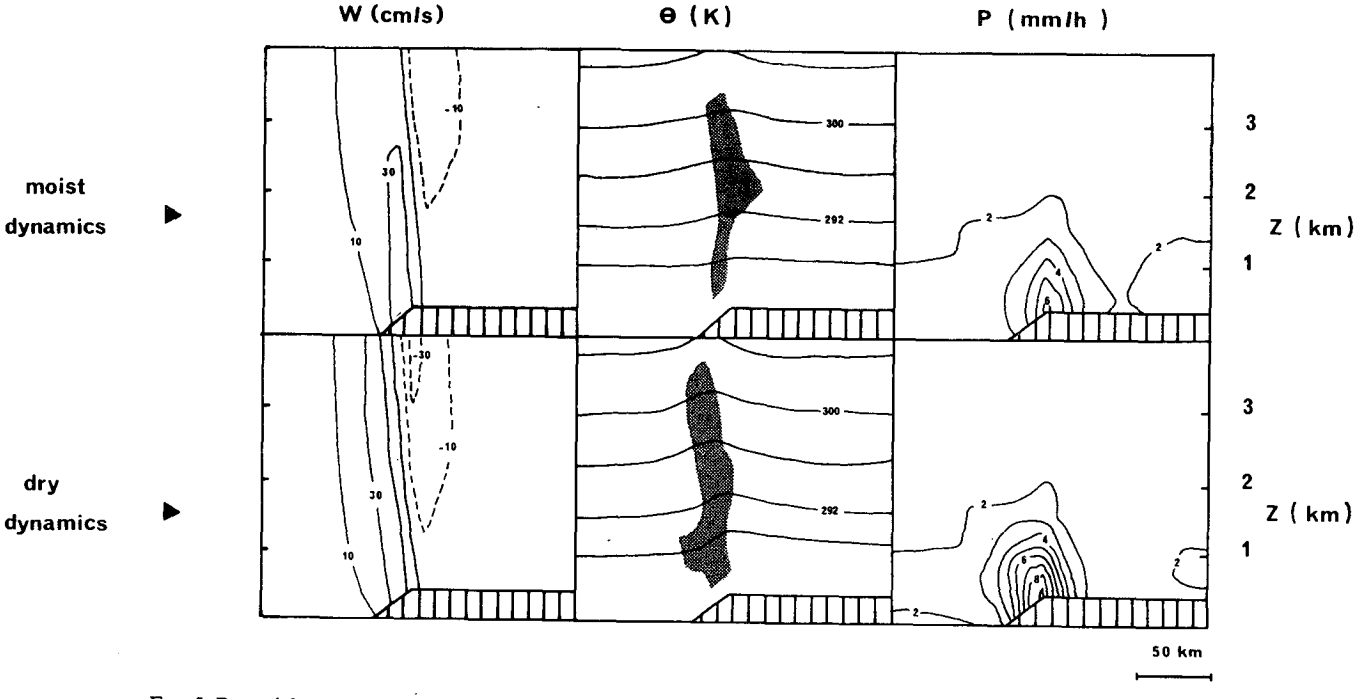

FIG. 5. Potential temperature and precipitation rate fields for a run with moist dynamics and a run with dry dynamics. The shaded area corresponds to the 0.1 g kg^{-1} contour of cloud water mixing ratio.

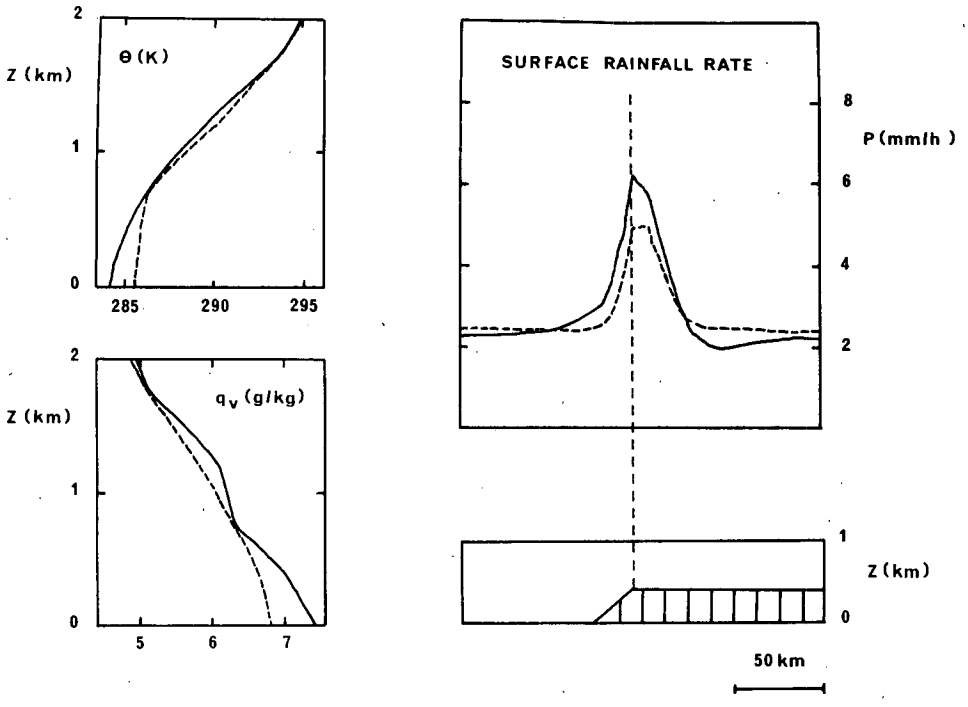

FIG. 6. Vertical profiles of potential temperature and vapor mixing ratio, and surface rainfall rate for a run with rain evaporation (solid line) and one without rain evaporation (dashed line).

d. Dynamical coupling

To investigate the role of the dynamical/microphysical interaction, experiment 5 was rerun with no coupling between the dynamics and the microphysics. In other words, in this experiment the dynamical fields behave just as they would in a dry simulation.

Vertical cross sections of vertical velocity, potential temperature and precipitation rate are displayed in Fig. 5 for the previously mentioned experiment 5 (referred to as moist dynamics), and for the new experiment (referred to as dry dynamics). In agreement with Durran and Klemp (1983), and Barcilon and Fitzjarrald (1985), the amplitude of the "dry" mountain wave is found to be larger than the moist one. Both vertical ascent and descent are stronger and larger in area in the case of dry dynamics, leading to a larger cloud over the crest and to a more intense evaporation over the plateau. The associated enhanced precipitation rates are significantly affected, since the maximum value of the "dry" case exceeds the one for the moist case by 3 mm h^{-1}.

e. Rain evaporation

Experiment 5 has also been rerun without the evaporation of the raindrops [Q_{eva} set equal to zero in Eqs. (1) and (2)]. As can be seen in Fig. 6, suppressing the rain evaporation reduces the precipitation rate at the hill crest by more than 1 mm h^{-1}. Evaporation acts to moisten and cool the upwind airflow, as is shown in the left part of Fig. 6, where the vertical profiles of potential temperature and vapor mixing ratio are displayed at a grid point located 60 km upwind to the crest. During the orographic lifting, condensation is favored and more cloud droplets are available to be washed out by the seeding raindrops. However, as expected, the surface precipitation rate past the crest and the orographic cloud is larger when the rain evaporation is turned off and the depletion—located about 50 km downwind of the crest and associated with the downdraft area—is no longer present.

4. Hill et al.'s cases

A detailed study of eight seeding events was presented by HBB. For each of them, HBB give upwind radiosounding as well as the field of the observed mean

TABLE 2. Computed cases for the observations of HBB.

Case no.	v_L (m s^{-1})	Z_s (km)	P_s (mm h^{-1})
1	30	2.2	2.5
2	28	1.5	1.5
3a	23	1.5	1
3b	26	1.5	1
4a	16	1.5	1
4b	22	1.5	1
4c	26	1.5	1
5	21	1.5	1
6a	19	1.5	1
6b	17	1.5	1
7a	14	1.5	1.5
7b	18	1.5	1.5
7c	21	1.5	1.5
8	14	1.5	3

rates of rainfall. Some of the events were subdivided according to the wind speed, thus yielding a total of 14 cases.

We attempted to simulate each of these different cases assuming a maritime type cloud spectrum and a seeding raindrop mean diameter of 100 μm. (We saw previously that an incorrect specification of these parameters should not significantly affect our results.)

Since little variability was observed in the vertical over the sea, HBB considered that the surface rainfall rate at a coastal site, P_0, was representative of the background precipitation rate associated with the seeder cloud. The seeding rate of rainfall was therefore taken from the coastal mean rainfall rate given in Fig. 12 of HBB, and we used the height of the corresponding contour above the hill as the seeding level in the model (usually 1.5 km except for case 1). The different parameters used for each simulation are listed in Table 2.

The computed precipitation fields for the eight cases are reported in Fig. 7. Each picture shows the value of the precipitation rate at the hill crest, P_h, as well as the coastal value, P_0. The circled value corresponds to the seeding precipitation rate, P_s. Just as in the observations, the vertical gradient of rainfall over the hills falls sharply from case 1 to case 8 as the mean wind speed decreases. The coastal value, P_0, is usually higher than the seeding value, P_h, this part of the domain having

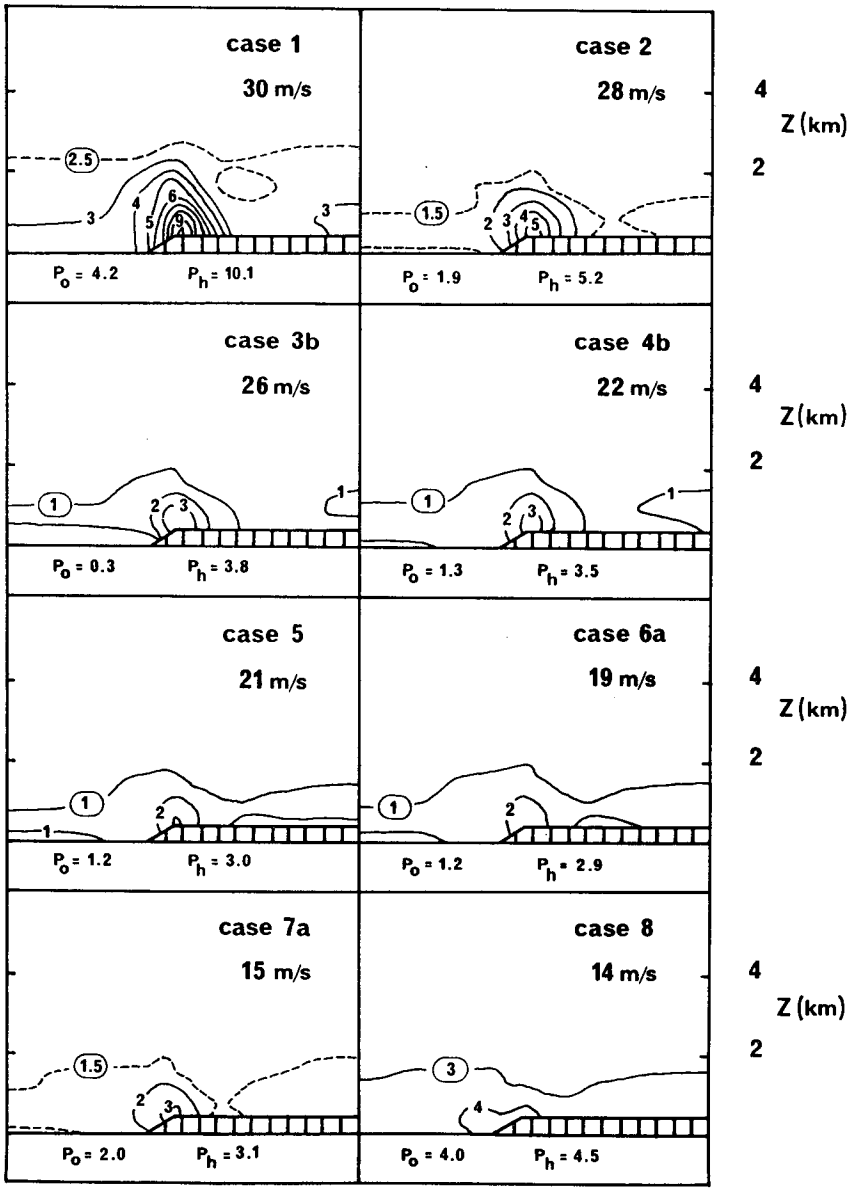

FIG. 7. Precipitation rate fields computed for the eight HBB observed cases. The circled contour corresponds to the seeding value.

already been modified by the orography. However, this is not always true. In case 3, for which the sounding is dryer than the others, P_0 is only 0.3 mm h^{-1} while the seeding value is 1 mm h^{-1}. The coastal value therefore may not always be representative of the seeding value.

In order to make a more quantitative comparison with the observations of HBB, we have plotted in Fig. 8 the computed enhancements from coast to hill, $P_h - P_0$, versus the observed values for all 14 cases. The agreement between computations and observations is reasonable for most of the cases. The underprediction of the enhancement in case 8 may be related to the presence of a strong shear in both wind speed and wind direction. A three-dimensional model might be more appropriate for this particular case.

In addition to the overall case-by-case agreement, the strong association between the enhancement from the coast to hill and the mean wind speed has been well reproduced by the model. Fig. 9 shows the behaviour of the curve of $P_h - P_0$ as a function of v_L as drawn by HBB, as well as our own curve. The results are quite similar.

To further investigate the dependence of orographic enhancement on wind speed and on the background rainfall intensity, P_s, an additional series of 12 experiments have been performed using the case 1 sounding. In these experiments the wind velocity was varied from 10 to 30 m s^{-1} and P_s from 1 to 4 mm h^{-1}, all other parameters being kept constant. The results of these calculations are displayed in Fig. 10 in the same format as the observations (see Fig. 15 of HBB). They reproduce the strong dependence of enhancement on wind speed, especially in the range 20 to 30 m s^{-1}. As in the observations, the dependence on P_s is much weaker

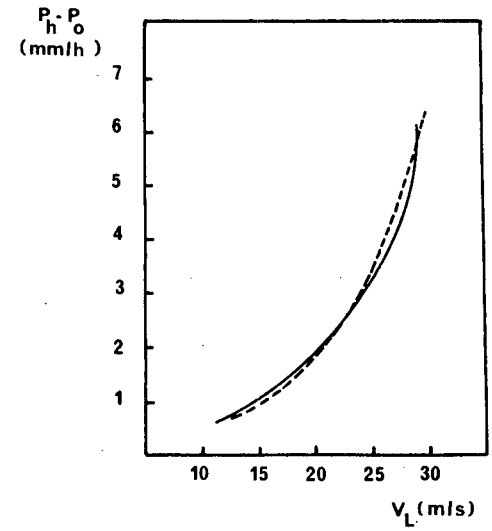

FIG. 9. Variation of the orographic enhancement, $P_h - P_0$, as a function of the mean low level wind speed, v_L: the results of HBB (dashed line) and our results (solid line).

and almost nonexistent for seeding rates above 2 mm h^{-1}. The rapid increase of the enhancement rate, as the wind speed increases from 20 to 30 m s^{-1}, is due mainly to the nonlinear dependence of the maximum vertical velocity upon the upstream airflow. Although our model does not predict the highest values of the observed enhancement (like $P_h - P_s > 6$ mm h^{-1}), the agreement with the observations is much better than the one obtained with the model of BR (results reported in Fig. 17 of HBB). This suggests that the observed sensitivity of the feeder-seeder mechanism to the wind speed is a result of nonlinear mountain wave dynamics and this effect cannot be accounted for by models with arbitrarily prescribed airflows.

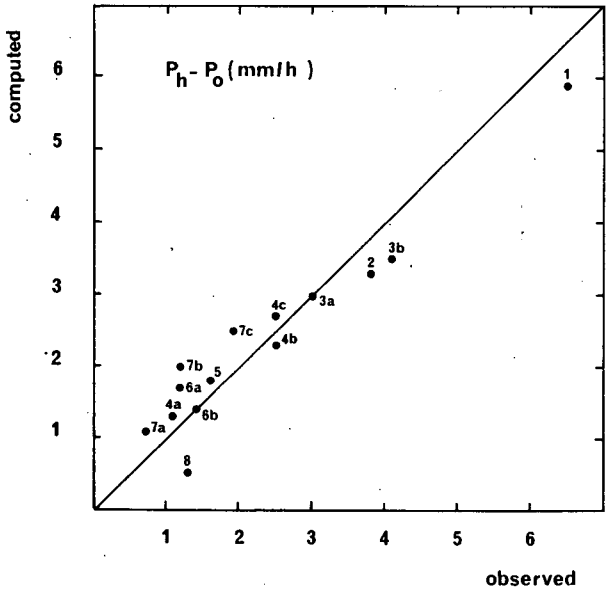

FIG. 8. Computed orographic enhancement, $P_h - P_0$, versus the observed one for the 14 cases.

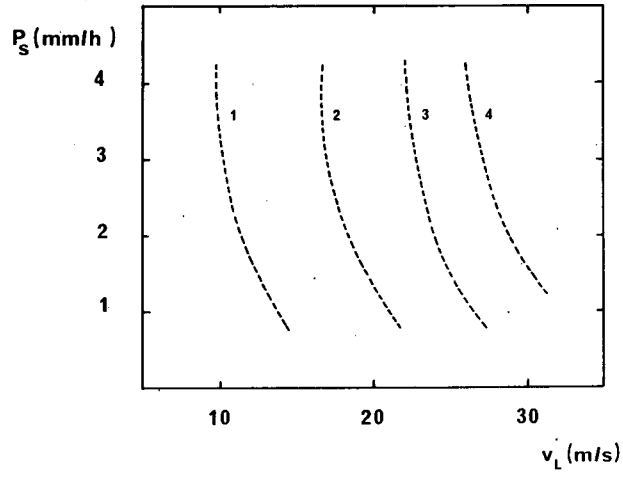

FIG. 10. Orographic enhancement, $P_h - P_0$, as a function of the seeding precipitation rate, P_s, and the mean wind speed, v_L.

5. Conclusion

The enhancement of precipitation which occurs when rain falls from an upper cloud layer into a lower orographically forced cloud has been simulated using a two dimensional version of a mesoscale model with parameterized microphysics. Initial soundings of wind, temperature and moisture, as well as rainfall data needed to verify the model prediction, are obtained from an observational study carried out in southern Wales. A case-by-case comparison has been made for each of 14 episodes and shows generally good agreement between model prediction and observed rainfall.

The orographic enhancement is found rather insensitive to microphysical parameters such as the cloud spectrum, the size of seeding raindrops or the preexisting precipitation rate, but the role played by the mountain wave dynamics appears to be dominant. Because of the nonlinear dependence of the maximum vertical velocity on the upstream horizontal flow, the orographic enhancement increases rapidly with the low-level wind speed. Moreover, the effect of moisture on the wave dynamics has to be considered: the presence of moisture, by reducing the stability, damps the dynamical response to the orographic forcing and consequently reduces the orographic enhancement. These effects cannot be well represented without an appropriate linking of the dynamics, thermodynamics and microphysics of moist mountain flow.

Acknowledgments. The authors would like to express their gratitude to P. Mascart and Prof. R. Rosset for their helpful comments and suggestions. They gratefully acknowledge J. Duron for computing assistance. The computer simulations were carried out with the support and assistance of CCVR, Palaiseau, France (Project No. 3857, 3951), ECWMF, Reading, England, and Météorologie Nationale, Paris. This work was funded by Electricité de France and the authors acknowledge their support.

APPENDIX

List of Symbols

D	raindrop diameter
D_{0r}	distribution parameter for the lognormal raindrop distribution
D_{0c}	distribution parameter for the lognormal cloud droplet distribution
$\overline{D_r}$	raindrop mean diameter (defined by $\rho_a q_{rw} = N_{rw}\rho_w \pi \overline{D_r}^3/6$)
$\overline{D_c}$	cloud droplet mean diameter (defined by $\rho_a q_{cw} = N_{cw}\rho_w \pi \overline{D_c}^3/6$)
$\overline{D_{sr}}$	mean diameter of the seeding raindrops
k_s	computational level at which seeding occurs
N_{rw}	raindrop number concentration
N_{cw}	cloud droplet number concentration
N_{aut}	autoconversion rate for the number concentration
N_{self}	self-collection rate for the number concentration
N_{sed}	sedimentation rate for the number concentration
P	precipitation rate
P_0	precipitation rate at the coast
P_h	precipitation rate at the hill crest
P_s	seeding precipitation rate
q	sum of water vapor and cloud water mixing ratios
q_v	water vapor mixing ratio
q_{cw}	cloud water mixing ratio
q_{rw}	rainwater mixing ratio
Q_{acc}	accretion rate for the mixing ratio
Q_{aut}	autoconversion rate for the mixing ratio
Q_{eva}	evaporation rate for the mixing ratio
Q_{sed}	sedimentation rate for the mixing ratio
S_N	sedimentation flux for the raindrop number concentration
S_q	sedimentation flux for the rainwater mixing ratio
var$x$	relative variance of the cloud spectrum
v_L	low-level wind speed
z_s	height at which seeding occurs
ρ_a	density of air
ρ_w	density of liquid water
σ_c	distribution parameter for the lognormal cloud droplet distribution
σ_r	distribution parameter for the lognormal raindrop distribution

REFERENCES

Bader, M. J., and W. T. Roach, 1977: Orographic rainfall in warm sectors of depressions. *Quart. J. Roy. Meteor. Soc.*, **103,** 269–280.

Barcilon, A., and D. Fitzjarrald, 1985: A nonlinear steady model for moist hydrostatic mountain waves. *J. Atmos. Sci.*, **42,** 58–67.

Bergeron, T., 1965: On the low-level redistribution of atmospheric water caused by orography. Suppl. Proc. Int. Conf. Cloud Phys., Tokyo, 96–100.

Carruthers, D. J., and T. W. Choularton, 1983: A model of the feeder-seeder mechanism of orographic rain including stratification and wind-drift effects. *Quart. J. Roy. Meteor. Soc.*, **109,** 575–588.

Durran, D. R., and J. B. Klemp, 1983: A compressible model for the simulation of moist mountain waves. *Mon. Wea. Rev.*, **111,** 2341–2361.

Gocho, Y., 1978: Numerical experiment of orographic heavy rainfall due to a stratiform cloud. *J. Meteor. Soc. Japan,* **56,** 405–423.

Hill, F. F., K. A. Browning and M. J. Bader, 1981: Radar and raingage observations of orographic rain over South Wales. *Quart. J. Roy. Meteor. Soc.*, **107,** 643–670.

Nickerson, E. C., E. Richard, R. Rosset and D. R. Smith, 1986: The numerical simulation of clouds, rain and airflow over the Vosges and Black Forest Mountain: a meso-β model with parameterized microphysics. *Mon. Wea. Rev.*, **114,** 398–414.

Storebo, P. B., 1976: Small-scale topographical influences on precipitation. *Tellus,* **28,** 45–59.